Transient Heat-Transfer Studies in Low Gravity Using Optical Measurement Techniques

Patricia J. Giarratano,* A. Kumakawa,† Vincent D. Arp‡
National Institute of Standards and Technology, Boulder, Colorado
and
Robert B. Owen§
Optical Research Institute, Boulder, Colorado

This paper summarizes heat-transfer measurements where a transient heat pulse in a metal surface induces a fluid velocity perpendicular to that surface. Surface temperatures are measured electrically and temperature profiles in the heated fluid are determined optically. A low-gravity environment is used to suppress gravitational convection. Diffuse-light holographic observations are shown to produce better fringe resolution than collimated-light interferometry within the heated boundary layer. Theoretical analysis is in excellent agreement with the electrical measurements, and satisfactory agreement with the optical measurements.

Nomenclature

A [m^2]	= metal cross section for current flow
c [m/s]	= velocity of sound in heat-transfer fluid
C_p,C_v [J/(kg-K)]	= fluid specific heats
C_{pm} [J/(kg-K)]	= metal specific heat
h [W/(m^2-K)]	= heat-transfer coefficient
K [W/(m-K)]	= fluid thermal conductivity
n [−]	= index of refraction
p [m]	= heat-transfer perimeter for area A
P [Pa]	= pressure
r [Ω-m]	= metal resistivity
(re) [m^3/kg]	= fluid refractivity
t [s]	= time
T [K]	= temperature of fluid
v [m/s]	= fluid velocity
x [m]	= distance perpendicular to the metal surface
z [m]	= distance parallel to the metal surface along the incident beam
ϕ [−]	= fluid Gruneisen parameter $= (1/\rho C_v)\,(\partial P/\partial T)_\rho$
ρ [kg/m^3]	= fluid density
ρ_m [kg/m^3]	= metallic density
θ [K]	= temperature of metal surface

Introduction

WHEN a pulse of heat is delivered from a solid surface into an adjacent compressible fluid, thermal expansion of the heated fluid generates a fluid motion. This induced fluid motion can perturb the heat-transfer process as compared to heat transfer to a fluid of constant density. Induced fluid motions corresponding to Reynolds numbers approaching 10^5 have been inferred from data on the stability of helium-cooled superconductors[1] in a confined geometry. For a given geometry, the thermally induced motions will be large when the thermal expansivity of the fluid is large, e.g., when the fluid pressure and temperature are somewhat close to the critical point. In zero gravity, the thermally induced motions may be dominant, whereas in the earthbound laboratory they are mixed with gravitational convection. Our work in this area is motivated by current interest in the use of near-critical fluids in heat-transfer processes.

Experimental studies of heat transfer from a solid surface to a surrounding fluid require the measurement of the temperatures of the solid surface and bulk fluid, and an applied heat flux. The addition of optical techniques to measure the fluid temperature field yields much more information with which to test models of the heat-transfer process.

Common optical techniques include interferometric, schlieren, and shadowgraph methods.[2-4] In these examples, the gradients of the index-of-refraction field, from which the temperature field of the fluid is obtained, are small enough that the optical records are easily interpreted. In this work, we extend the heat-transfer process to include large, time-varying, nonuniform gradients of refractive index. We compare Mach-Zehnder interferometry using a collimated light source with holographic interferometry using a diffuse light source.

A series of tests in the NASA KC-135 aircraft, which stimulates conditions of low gravity, have eliminated gravitational convection, enabling us to relate the observed gradient unambiguously to thermally induced convection.[5] Heat-transfer results are tested against a one-dimensional model of heat transfer to a compressible fluid.

Mathematical Model for Heat-Transfer-Induced Velocity

In a one-dimensional coordinate system normal to heated surface, mass, momentum, and energy balance in a fluid are represented by the following[6,7]

$$\frac{\partial v}{\partial t} = -v\frac{\partial v}{\partial x} - (1/\rho)\frac{\partial P}{\partial x} \tag{1}$$

$$\frac{\partial P}{\partial t} = -v\frac{\partial P}{\partial x} - \rho c^2\frac{\partial v}{\partial x} - \phi K\frac{\partial^2 T}{\partial x^2} \tag{2}$$

$$\frac{\partial T}{\partial t} = -v\frac{\partial T}{\partial x} - \phi T\frac{\partial v}{\partial x} + (1/\rho C_v)K\frac{\partial^2 T}{\partial x^2} \tag{3}$$

Presented as Paper 88-0346 at the AIAA 26th Aerospace Sciences Meeting, Reno, NV, Jan. 11-14, 1988; received Feb. 4, 1988; revision received Oct. 20, 1988.

*Mechanical Engineer, Chemical Engineering Science Division.
†Physicist, Chemical Engineering Science Division. From the National Aerospace Laboratory, Miyagi, Japan.
‡Physicist, Chemical Engineering Science Division.
§President.

It is important to note that these equations do not include viscous dissipation, and that they are valid for any single-phase fluid state, including the near-critical region. In an open system, where the pressure is essentially constant, these reduce to

$$\frac{\partial T}{\partial t} = -v\frac{\partial T}{\partial x} + (K/\rho C_p)\frac{\partial^2 T}{\partial x^2} \tag{4}$$

$$\frac{\partial v}{\partial t} = -(\phi K/\rho c^2)v\frac{\partial^2 T}{\partial x^2} \tag{5}$$

If the velocity terms are neglected, the equations reduce to those for classical thermal diffusion, though near the fluid critical point the diffusivity may be a strong function of position through its dependence on density and temperature. Retaining the velocity terms, but assuming the fluid diffusivity is constant, a simple analytical solution to Eqs. (4) and (5) is found:

$$v(x=\infty) = (\phi/\rho c^2)\cdot q(x=0) \tag{6}$$

This analytical solution can be used to test the accuracy of the computer calculation for this special case.

Boundary conditions at $x = 0$ (the heated surface) are determined from the equation

$$i^2 r/A = \rho_m c_{pm} A\frac{d\theta}{dt} + hp(\theta - T) \tag{7}$$

The terms represent, respectively, Joule heating, temperature rise of the metallic heater, and heat transferred to the fluid (by fluid conduction) at the heater surface.

An example of a large change in the calculated temperature profiles from inclusion of the velocity terms is shown in Fig. 1, for helium near its critical point.[8]

For the following experimental work, numerical solutions to Eqs. (4) and (5) are obtained using properties data from an equation of state for the experimental fluid, Refrigerant-13.[9]

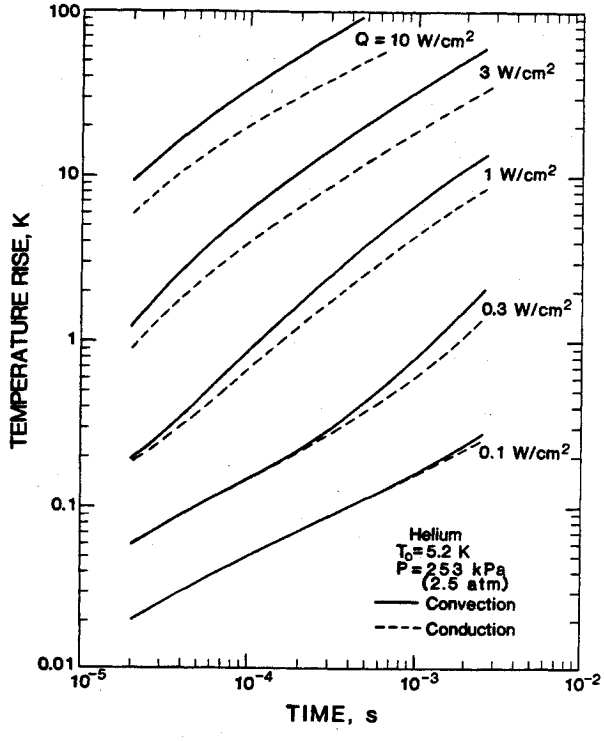

Fig. 1 Surface temperature changes as a function of time for several impulsive heat fluxes, calculated assuming simple conduction (dashed lines) and induced convection (solid lines).

For a given heat pulse, output from the calculations above includes the fluid density as a function of time and distance from the heated surface. Then, using the Lorentz-Lorenz law, the refractive index is calculated, also as a function of time and distance. This refractive index profile is an output to the subsequent ray-tracing calculation (described below) of the optical paths through the boundary layer.

Ray Tracing

The deflection of the optical beam is then determined by integrating

$$d^2x/dz^2 = [1 + (dx/dz)^2](1/n)(dn/dx) \tag{8}$$

along the optical path for the given incident ray. Boundary conditions are $x = x_0$ and $dx/dz = 0$ at $z = 0$, representing an incident beam at height x_0 above, and parallel to, the heater surface. We then trace this beam until it leaves the heated region, knowing $n(x)$ and dn/dx from the heat-transfer calculations above. Next, integration along the optical path to the plane surface, which records either the Mach-Zehnder interferogram or the hologram, allows us to calculate the expected interference with a reference optical beam.

Experimental System

The test cell used in the study is shown in the photograph in Fig. 2. The electric heater surface, magnified in the lower portion of the photograph, was a titanium strip 0.058 mm thick, 27.2 mm long, and 4.57 mm wide. Its electrical resistance as a function of temperature was calibrated separately. In the heat-transfer experiments, the electrical resistance of the titanium was recorded during the passage of the electrical current pulse; this provided both the power input and the surface temperature as a function of time. A thermistor measured the bulk temperature of the Refrigerant-13, the

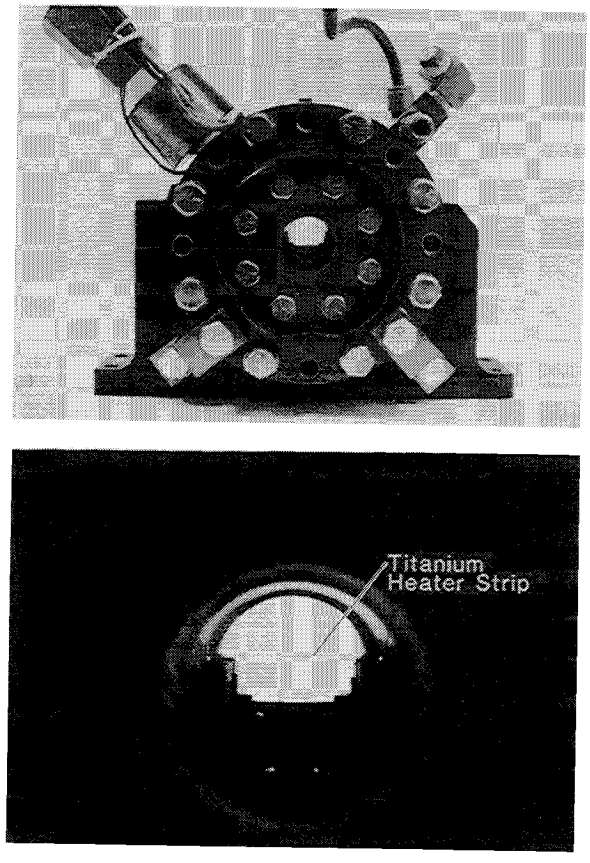

Fig. 2 Experimental test cell.

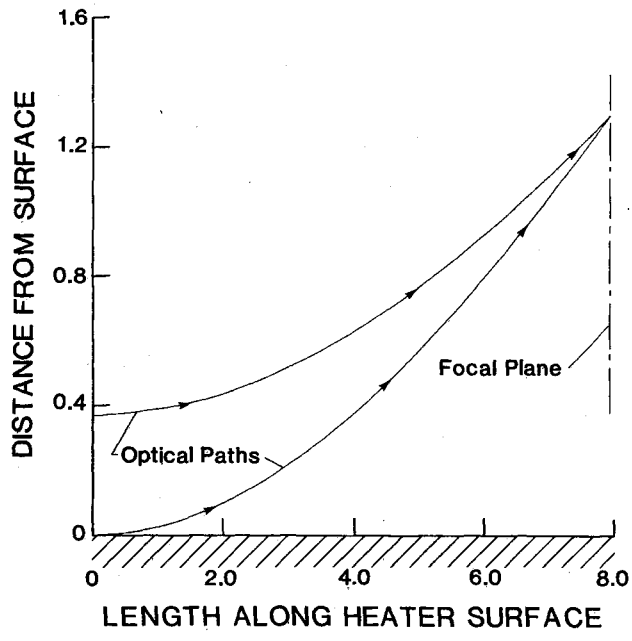

Fig. 3 Calculated optical paths for two different incident rays which converge to the same point in the optical plane (object plane). Lengths are normalized by the boundary-layer thickness.

heat-transfer fluid, at a point several centimeters from the heated surface. Simultaneously, interferograms of the temperature field in the fluid adjacent to the heater were recorded.

Optical Techniques

Optical techniques use the following relation between refractive index n and density (or temperature, for a known pressure) to obtain direct measurements of temperature gradients in the fluid for Refrigerant-13:

$$n = \frac{1-\rho(re)}{1+2\rho(re)}; \qquad (re) = 1.13 \times 10^{-4}\ \mathrm{m^3/kg} \qquad (9)$$

In most previous applications, the thermal and refractive index gradients in the field of view were small and the optical results easily interpreted. However, in the present study, the large, time-varying, nonuniform refractive index gradients in the boundary layer are sufficient to render many classical techniques, such as Mach-Zehnder interferometry, inadequate for quantitative studies.

With collimated incident light, used with Mach-Zehnder interferometry, we can find a limiting refractive index gradient above which fringes disappear entirely in a plane geometry. This disappearance occurs when more than one deflected light ray reaches the same image point in the recording system. Figure 3 shows two different ray paths, both initially parallel to the heater surface, converging to a single point in the focal plane of the viewing lens. The paths were calculated numerically, as described above, using dimensions normalized by the boundary-layer thickness. An end correction, where the fluid temperature gradient is not parallel to the sample surface, is neglected.

Holographic interferometry permits the use of a diffuse sample beam and thereby eliminates some of the problems caused by the collimated team (required by the Mach-Zahnder technique). Indeed, under high gradients where it was not even possible to image the actual titanium strip using Mach-Zehnder configurations, the strip was clearly visible in the diffuse-light hologram. This is because the shadowgraph effects associated with collimated incident light disappear when diffuse incident light is used. Further, it proved to be possible in the laboratory to observe fringes in the outer three-quarters of the depth of the boundary layer. However,

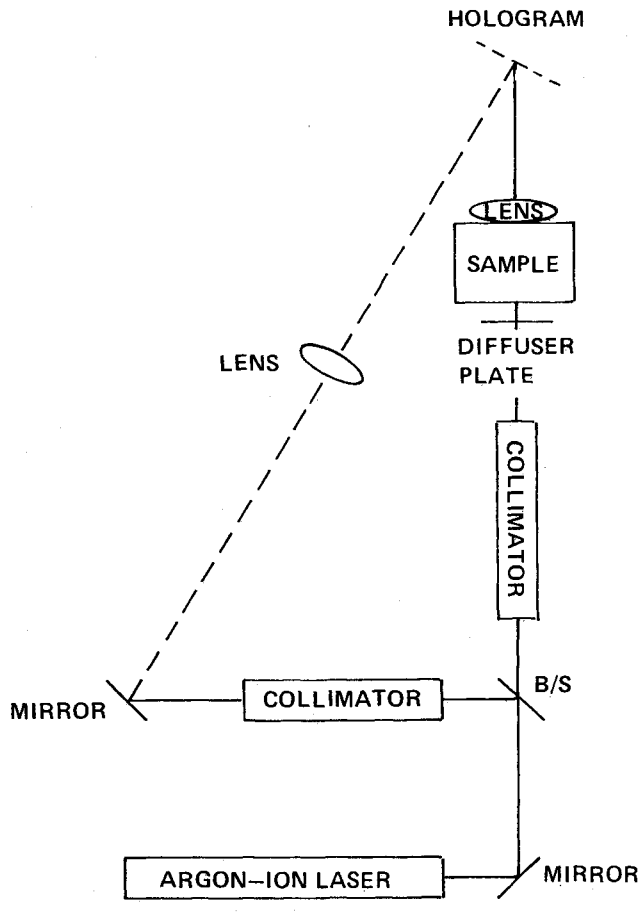

Fig. 4 Optical layout of the holographic microscopy system.

the computer model described above indicated that a typical boundary layer would contain about 50 fringes, with most of them being packed next to the heater. Hence, even with the holography, both theoretical as well as practical resolution limits are exceeded as we approach very close to the surface. Tomographic techniques,[10] which we have not tried, would probably be equally unusable in this limit.

The measurements were performed using double-exposure holography. It was important to make the individual exposures as short as reasonably possible in order to minimize the temperature variation during each exposure interval. In the laboratory, each individual exposure was 1 ms in duration and the time between double exposures was controlled to within 1 ms. This was accomplished by limiting the size of the holograms to 1–2 cm in diameter and by using a 3 W argon-ion laser as a light source. This arrangement had a high enough optical power density in the recording plane to allow the use of high resolution holographic plates for the holograms, which further aided in the final spatial resolution.

A test run consisted of the application of an approximately square-wave current pulse through the heater for 0.4 s to 1.0 s, depending on the applied electrical power level. The first 1 (or 5) ms holographic exposure was made simultaneously with the start of the pulse, with a second 1 (or 5) ms exposure being made later. Time delays between exposures ranged from 30 to 200 ms in the laboratory, and up to 900 ms in zero gravity. The double-exposure sequence was timed by an exposure controller which had the required 1 ms time resolution. The system layout is shown schematically in Fig. 4.

Low-Gravity Measurements

The NASA KC-135 aircraft flies a series of parabolic maneuvers, each of which yields approximately 25 s of low-gravity conditions. During each low-g period, the apparent

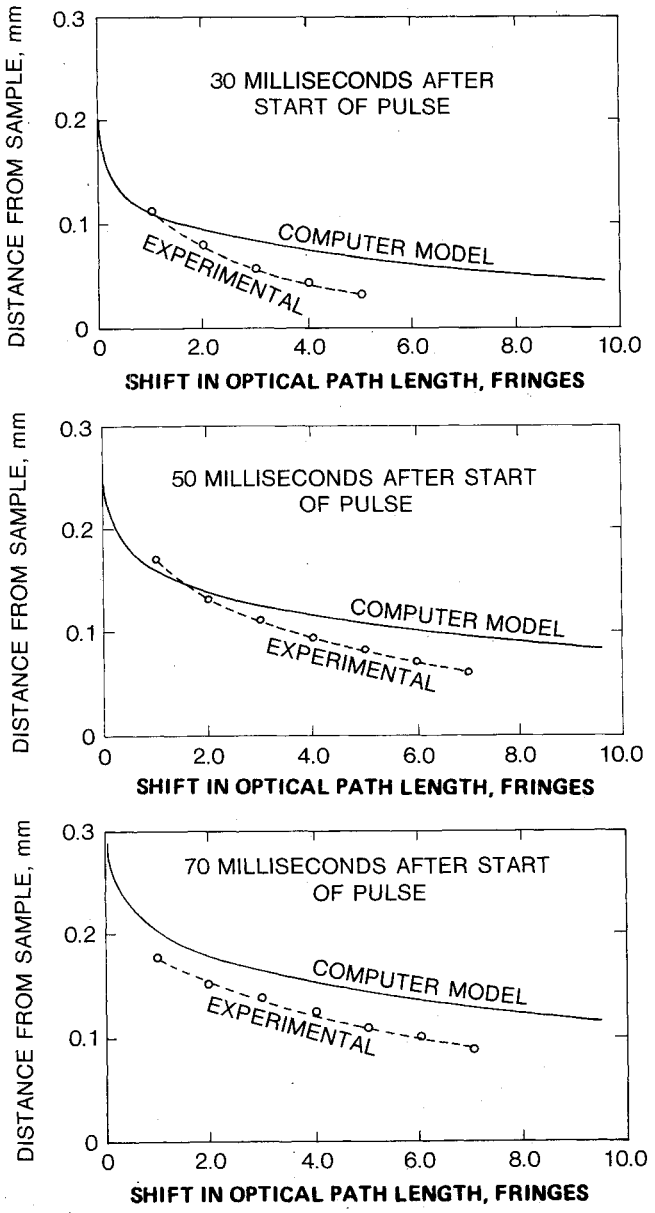

Figs. 5–7 Comparison between calculated and experimental values of fringes in the thermal boundary layer.

gravitational force is roughly 0.01 that normally experienced at sea level.

The low-gravity measurements were considerably less refined than those made in the laboratory, primarily due to the impracticality of using the laboratory argon-ion laser on board the KC-135. In flight, a 20 mW He-Ne laser was used. Although this laser performed well under low-gravity conditions, the decrease in power greatly increased the exposure times, making it impossible to utilize the high-resolution holographic emulsion which was used in the laboratory. The aircraft's optical system was mounted on an optical breadboard which was isolated from aircraft vibration by rubber shock mounts. Nevertheless, because of residual vibrations it was necessary to restrict exposure times to 5 ms or less in order to successfully record a hologram.

While it might be possible to increase this time through the use of air vibration isolation systems, the apparent gravity loading cycle encountered during a typical low-g parabola makes the design of such a system nontrivial. Since a longer exposure time would also be contrary to the short measurement time desired to record the transient phenomenon of interest, rather than attempt to design a low-g compatible air-isolation system, we used high-speed holographic recording material. The incorporation of this emulsion into the aircraft optical system lowered the exposure time to 5 ms per exposure for a double-exposure hologram. However, there was a noticeable loss in image resolution. We therefore decided to maximize spatial resolution through use of holographic microscopy, with the realization that only the outer part of the layer could be probed. However, the loss of resolution was such that fringe patterns were only occasionally observable, and the main analysis has been restricted to the very outer parts of the boundary layer.

Results from Optical Measurements

The holographic images were reconstructed for fringe analysis. In the laboratory measurements, the 100 and 200 ms delays showed significant gravity-driven convection in the boundary layer, so detailed thermal profiles were not calculated for those cases. In the KC-135 aircraft, simulated low-g conditions were such that gravity-driven convection was not observed in the boundary layer for long delay times, so it proved possible to separate the exposures by many hundreds of milliseconds. The experimental time was thus limited by possible burnout of the heater at high temperatures.

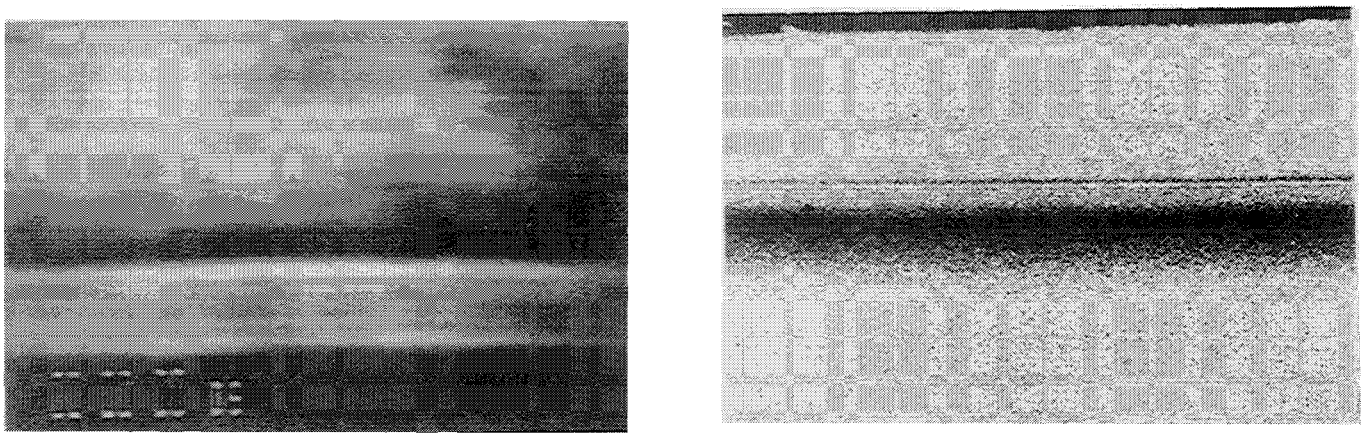

Mach-Zehnder Interferogram **Double-Exposure Holographic Interferogram**

Time: 50 milliseconds after start of pulse, boundary layer thickness: 0.2 mm

Fig. 8 Comparison of Mach-Zehnder and holographic images of the transient heat-transfer boundary.

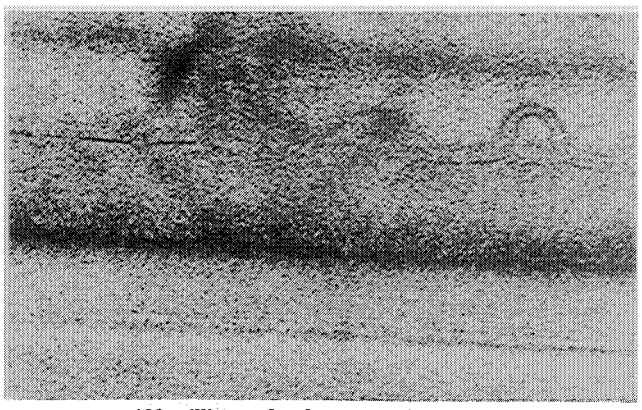

100 milliseconds after start of heat pulse

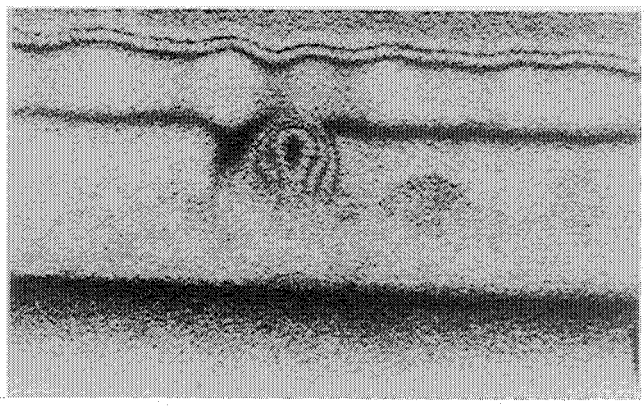

200 milliseconds after start of heat pulse

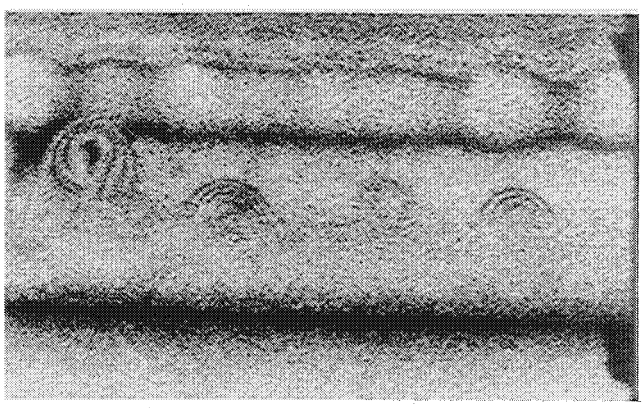

200 milliseconds after start of heat pulse

Fig. 9 Holographic interferograms of boundary-layer convective cells.

The results from laboratory double-exposure holography are shown in Figs. 5–7. Approximately three-quarters of the boundary layer can be probed holographically, and this measurement range can be extended further by extrapolation, since the heater temperature itself is measured electronically and provides a reference point. However, we do find a discrepancy between theory and the observed fringe locations, which is unexplained at this time.

The time and spatial resolution of the laboratory experimental arrangement proved to be excellent, with 1 ms time resolution and 0.02 mm fringe spatial resolution being achieved. A direct comparison of a typical hologram with a typical Mach-Zehnder measurement of the same sample is shown in Fig. 8. The double-exposure hologram shows an obvious improvement; in the Mach-Zehnder photograph it is not even possible to accurately locate the heater strip. This improvement is credited primarily to the use of a diffuse object beam in the holographic arrangement. It was also possible to observe flow cells outside the boundary layer after the onset of gravity-driven convection (Fig. 9).

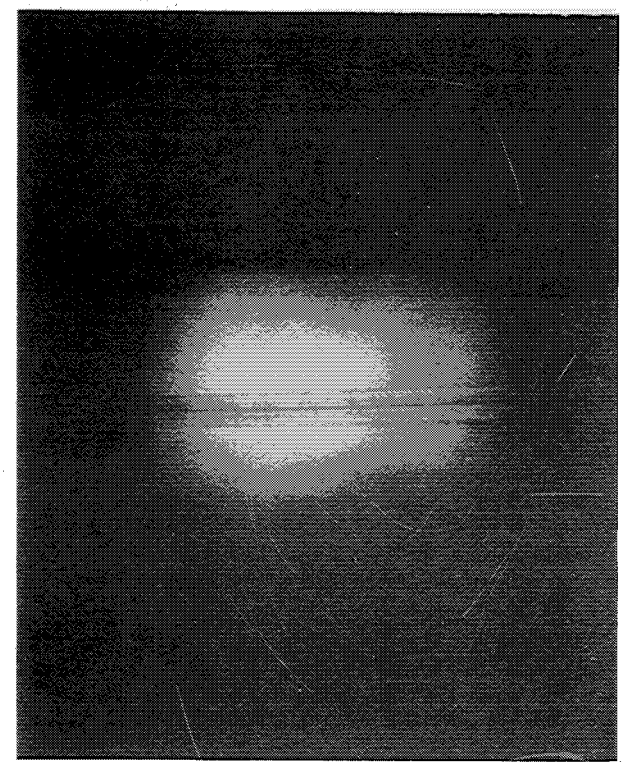

Fig. 10 Reconstructed image from hologram of thermal boundary layer in low-gravity, 800 ms after start of pulse.

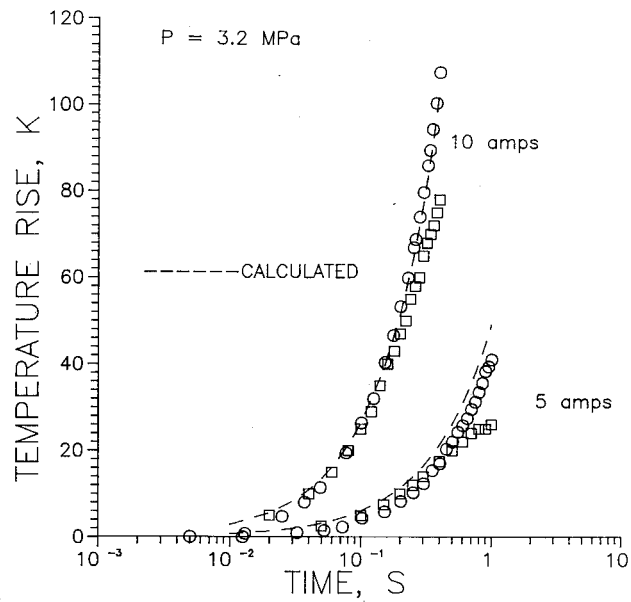

Fig. 11 Heater surface temperature rise in low gravity (circles) and 1*g* (squares).

Similar improvements over classical Mach-Zehnder interferometry were observed in the low-*g* holograms. However, analysis was restricted due to poor fringe resolution. The reconstructed image from a typical low-*g* hologram is shown in Fig. 10.

Results from Electrical Measurements

An example of the heater surface temperature rise during a heat pulse, as measured by the electrical resistance, is shown in Fig. 11. The figure compares the KC-135 data (low-*g*) and ground data (1-*g*). As expected, the low-*g* data agree with the

surface temperature as determined from the computer model; the model accounts for the thermally induced motion but not gravity-driven motion. The deviation of the 1-g data from the calculated curve occurs at the onset of natural convection due to buoyancy forces.

Conclusions

Holographic interferometry with a diffuse light source is a useful optical technique for measuring temperature profiles in thin boundary layers with very steep temperature gradients, such as may exist in transient heat transfer from a heater surface to highly compressible fluids. The technique offers significant improvement over classical methods, such as Mach-Zehnder interferometry, which is limited by refraction and shadowgraph effects.

The primary limitations of the holographic technique are the fringe resolution limits of holographic recording materials and the exposure times necessary to record the hologram during a transient heat pulse; for these experiments the duration of the heat pulse was 1 s or less. With sufficient laser power available and proper microscopy imaging, these limitations can be minimized.

The initial tests in a low-gravity environment, where thermal boundary-layer temperature profiles were measured during a heat pulse, have provided evidence that the computer model describing the transient heat transfer is correct. Further low-gravity tests are needed to optimize the optical measurement technique and better substantiate the computer model.

References

[1]Arp, V., and Persichetti, J. M., "Thermally-induced Flow in a Confined Fluid," *International Communications in Heat Mass Transfer*, Vol. 14, 1987, pp. 567-576.

[2]Eckert, E. R. G. and Soehngen, E., "Interferometric Studies on the Stability and Transition to Turbulence of a Free Convection Boundary Layer," Proceedings of the General Discussion Heat Transfer, Inst. of Mechanical Engineers, American Society of Mechanical Engineers, London, U.K., 1951.

[3]Hauf, W. and Grigull, U., "Optical Methods in Heat Transfer," *Advances in Heat Transfer*, Vol. 6, edited by J. P. Hartnett and T. F. Irvine, Jr., Academic, New York, 1970, pp. 133–136.

[4]Goldstein, R. J., "Optical Techniques for Temperature Measurements," *Measurements in Heat Transfer*, edited by E. R. G. Eckert and R. J. Goldstein, McGraw-Hill, New York, 1976, pp. 241–293.

[5]Owen, R. B., Giarratano, P. J., and Arp, V. D., "The Use of Holography to Measure Heat Transfer in High Gradient Systems," Optical Society of America 1986 Annual Meeting, Seattle, WA, Oct. 1986. Abstract: JOSA 3A Series 2, P113, 1986.

[6]Arp, V., "Thermophysics of Single-Phase One-Dimensional Fluid Flow," *Cryogenics*, Vol. 15, May 1975, pp. 285–289.

[7]Arp, V., Chen, G.-B., and Persechetti, J. M., "The Gruneisen Parameter in Fluids," *Journal of Fluids Engineering*, Vol. 106, June 1984, pp. 193–201.

[8]Daney, D., National Institute of Standards and Technology, Boulder, CO, unpublished.

[9]Chan, C. Y. and Haselden, G. G., *International Journal of Refrigeration*, Vol. 4, 1981, p. 131.

[10]Cha, S. and Vest, C. M., "Tomographic Reconstruction of Strongly Refracting Fileds and Its Application to Interferometric Measurement of Boundary Layers," *Applied Optics*, Vol. 20, 1981, pp. 2787–2794.